Direct Photomodification of Polymer Surfaces: Unleashing the Potential of Aryl-Azide Copolymers

*Anita Schulz, Antonio Stocco, Audrey Bethry, Jean-Philippe Lavigne, Jean Coudane, Benjamin Nottelet**

Dr. Anita Schulz, Audrey Bethry, Prof. Jean Coudane, Dr. Benjamin Nottelet
IBMM, Université de Montpellier, CNRS, ENSCM, Montpellier, France.
E-mail: Benjamin.Nottelet@umontpellier.fr
Dr. Antonio Stocco
L2C, Université de Montpellier, CNRS, Montpellier, France.
Prof. Jean Philippe Lavigne
INSERM unité 1047, Université de Montpellier, Nîmes, France; Service de microbiologie, CHU Caremeau, Nîmes, France.

Keywords: photochemistry, poly(2-oxazoline)s, antibacterial, polymer surface, aryl-azide

Abstract

The possibility to impart surface properties to any polymeric substrate using a fast, reproducible and industrially friendly procedure, without the need for surface pre-treatment, is highly sought after. This is in particular true in the frame of antibacterial surfaces to hinder the threat of biofilm formation. In this study we demonstrate the potential of aryl-azide polymers for photo-functionalization and the importance of the polymer structure for an efficient grafting. The strategy is illustrated with a UV-reactive hydrophilic poly(2-oxazoline) based copolymer, which can be photografted onto any polymer substrate that contains carbon-hydrogen bonds to introduce antifouling properties. Through detailed characterization it is demonstrated that the controlled spatial distribution of the UV-reactive aryl-azide moieties within the poly(2-oxazline) structure, in the form of pseudo gradient copolymers, ensures higher grafting efficacy than other copolymer structures including block copolymers. Furthermore, it is found that the photografting results in a covalently bound layer, which is thermally stable and causes a significant anti-adherence effect and biofilm reduction against *E. coli* and *S. epidermidis* strains while remaining non-cytotoxic against mouse fibroblasts.

1. Introduction

The assembly of microbial cells within a self-produced extracellular matrix of proteins, polysaccharides, nucleic acids and lipids on a surface is a quickly occurring and highly undesirable process known as biofilm formation. Biofilm causes many problems in very diverse fields of applications: in the container-shipping industry it adds weight and friction, in the oil and water desalination industry it blocks filtration and causes corrosion, in the food industry it contaminates and in hospitals it is responsible for almost half of the hospital acquired infections and sometimes even death.[1-3] The relevance of this problem is reflected in the numerous approaches to obtain antibacterial surfaces. Such antibacterial surface properties can be achieved through bioactive or biopassive surface modifications.[4,5] Bioactive coatings kill bacteria upon approach e.g. through positive charges or by releasing substances such as antimicrobial agents or silver ions. The activity can be hampered over time though, due to limited release of the substances or the deposition of dead bacteria on the surface. More importantly the release of antimicrobial agents can cause the emergence of resistant strains of bacteria. In contrast, biopassive strategies prevent the adhesion of bacteria on the surface, but are not bactericidal. Such a biopassive surface modification can be realized through the employment of hydrophilic graft polymers with anti-fouling properties. These polymers can be attached either through a *grafting from* (polymerization from the surface) or through a *grafting onto* (functional polymer grafted to the surface) approach. Both grafting methods have their merits and drawbacks, but in general require reactive groups either on the surface, in the graft polymer or both. Here versatile chemical motifs, such as organosilanes, which attach to various metal surfaces, are essential tools to introduce functional groups or graft polymers directly to the substrates. In recent years, mussel adhesive proteins and their peptide mimics have also gained increased interest, since they not only attach to multiple metal surfaces, but also to polymer substrates.[6,7] However their attachment is based on intermolecular forces such as hydrogen bonding, electrostatic and hydrophobic interactions

and π- π stacking, but not covalent bonds.[6] In order to achieve covalent conjugation to polymer substrates, the surface has to be activated, often via complex and time-consuming chemical reactions, which can even lead to degradation of the surface material. In addition, such surface activation processes and the subsequent functionalization are often tailored to the chemical composition of the surface and not conferrable to other surface materials. This was in fact, illustrated by our recent work where a "surface preactivation / grafting to" approach was successfully reported to yield potent antibacterial polyester surfaces.[8,9] Despite efficient, non-degrading and biocompatible click ligation strategies, in particular thiol-yne photoaddition, the main disadvantage was the required preactivation step that was only applicable to aliphatic polyesters, thus limiting the potential of the approach to a family of polymer substrates.

To overcome this limitation and with aim to provide flexible and versatile surface modification on a wide range of polymer substrates, we focus in this work on UV-activated nitrene species. It is well known, that nitrenes can insert into carbon-hydrogen bonds, a common chemical entity in most polymer substrates. Here aryl-azides have proven to be very stable precursors, which photolyse efficiently into the reactive nitrene species.[10] Already in 1969 an aryl-azide derivative was utilized as a labeling reagent for an antibody by Fleet et al.[10] Since then aryl-azides have been used for various applications, such as radioactive labeling of phospholipids,[11,12] crosslinking of polymer chains,[13] and introduction of functional groups on substrates,[14,15] and in polymer chains.[16,17] Interestingly though, despite its versatility, the exploitation of this photoreactive moiety remained scarce over the last decades to directly graft UV-reactive polymers chains onto most polymeric surfaces. Zhu et al. reported on aryl-azide chitosan/heparin complexes to inhibit platelets adhesion and activation.[18] Li et al. described fluorinated acrylate copolymers for hydrophobization of fabrics.[19] Hadler et al. investigated the photochemical modification of polyimide Kapton®

substrates with various hydrophilic polymers, which were functionalized with aryl azide groups in a post analog reaction.[20] However, in all cases the aryl-azide moieties were randomly embedded in the polymer chain and polymer block, respectively. It is our belief that this lack of exploitation is mainly due to the absence of systematic study dedicated to the repartition of aryl-azide moieties in the polymer chains and its influence on the photografting efficiency. To the best of our knowledge, this approach has never been investigated before to realize antibacterial surfaces using a pseudo gradient or block aryl-azide containing antifouling copolymer exhibiting a controlled spatial distribution of the aryl-azide moieties for an efficient surface anchoring (**Figure 1A**).

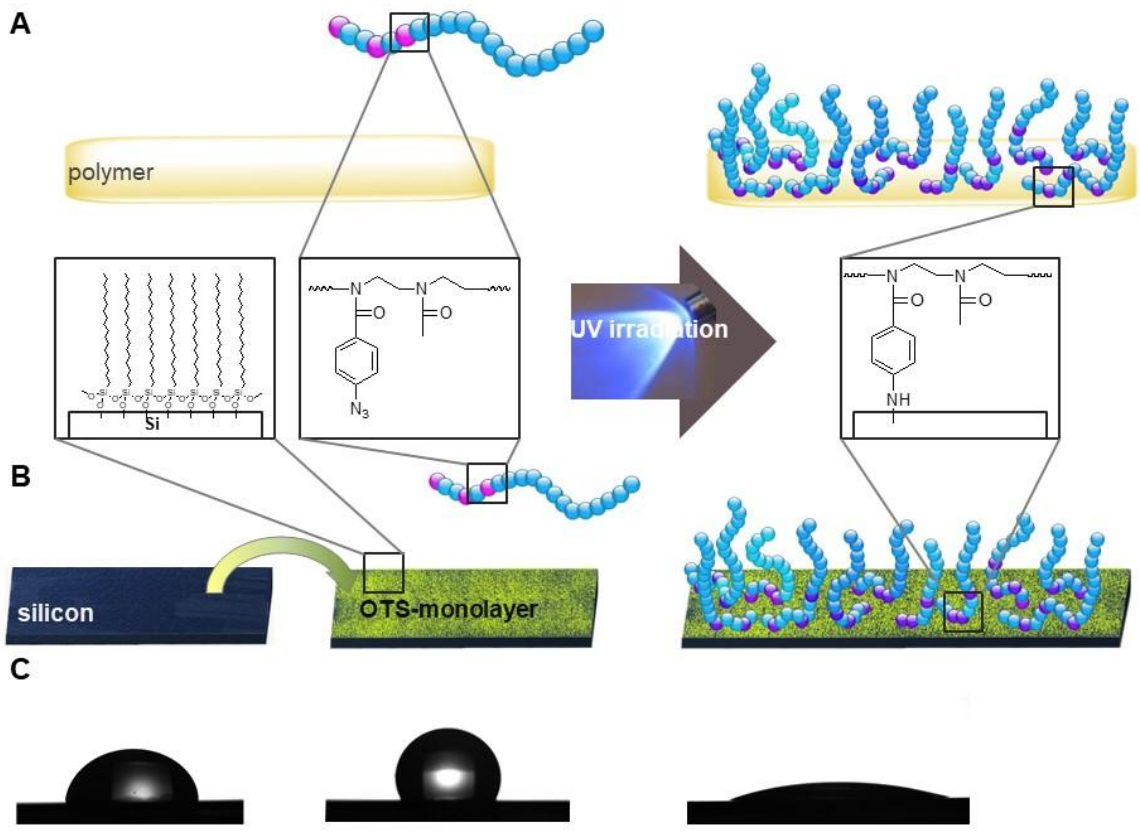

Figure 1. Schematic illustration of the grafting process of poly(2-oxazoline) copolymers onto polymer substrates (A) and OTS-monolayer deposited on silicon wafer (B) with the help of UV irradiation. Static water contact angles (C) are shown for silicon (left), OTS-monolayer (middle) and grafted poly(2-oxazoline) layer (right).

2. Results and Discussion

2.1 Photoinsertion of copolymers bearing a single aryl-azide chain-end moiety

To introduce aryl-azide groups with control over quantity and location in the polymer structure, living polymerization is the method of choice. Initially, we used an aryl-azide bearing initiator, 4-azidoaniline (AzPh), for the living ring-opening polymerization of sarcosine-*N*-carboxyanhydride (Sar-NCA) to ensure that each polymer chain featured one aryl-azide moiety at the chain end. The resulting polymer, polysarcosine (PSar), is also more and more recognized as an interesting alternative to polyethylene glycol (PEG), the current standard for antifouling coatings.[21,22]

Methanolic solutions of the polymer (c=10 or 20 g/L) were spray-coated on polypropylene (PP) and poly(lactic acid) (PLA) substrates, which were warmed to 50-60°C to ensure quick evaporation of the solvent. The substrates were exposed to UV light by placing it under a chromatography lamp (254 nm, 8W) at a distance of approx. 3 cm for 20 min. The coating step was repeated up to five times, with in between washing steps, to remove UV-deactivated polymer chains from the surface. While the emergence of a nitrogen peak in X-ray photoelectron spectra (XPS) confirmed the attachment of AzPh-PSar on PP (**Figure 2**) and PLA substrates (**Figure S1**), water contact angle measurement did not show an increase of the surface energy (PP: 103°→97°; PLA: 67°→ 68°; 10g/L, AzPh-PSar$_{100}$). This absence of improvement was attributed to the inherent roughness of the substrates surfaces conferred by the hot-plate press process used to prepare the PP and PLA substrates.[23]

Thus, as a model system, a silicon wafer with an octadecyltrichlorosilane (OTS) monolayer (Figure 1B), was employed to facilitate a more suitable surface characterization. Here, the water contact angle of the surfaces dropped from ~105° with just the OTS monolayer to ~80° after multiple coating steps. This drop was caused by a grafted polymer layer of only a few nm thickness as determined by ellipsometry measurements (**Table 1**).

Table 1. Overview of various parameters (polymer structure, concentration and irradiation time) and their influence on the grafting efficacy expressed in layer thickness and static water contact angle (OTS-monolayer deposited on silicon wafer used as model substrate).

polymer	conc. [g/L]	irradiation time [min]	thickness [nm]	static contact angle[a] [°]
AzPh-PSar$_{10}$	20	5 x 20	2.1 ± 0.2	83 ± 9
AzPh-PSar$_{100}$	20	5 x 20	0.9 ± 0.1	82 ± 9
P(AzPhOx)$_5$-*b*-(MeOx)$_{100}$	10	5 x 20	0.5 ± 0.6	54 ± 6
P(AzPhOx)$_5$-*b*-(MeOx)$_{100}$	20	5 x 20	1.7 ± 0.5	53 ± 15
P[(AzPhOx)$_5$-*co*-(MeOx)$_{10}$]-*b*-(MeOx)$_{90}$	10	1 x 20	11.8 ± 0.9	63 ± 8
P[(AzPhOx)$_5$-*co*-(MeOx)$_{10}$]-*b*-(MeOx)$_{90}$	10	5 x 20	13.6 ± 2.2	33 ± 12
P[(AzPhOx)$_5$-*co*-(MeOx)$_{10}$]-*b*-(MeOx)$_{90}$	20	5 x 20	5.5 ± 0.3	40 ± 7

[a] Data is represented as means±SEM (n=3).

2.2 Photoinsertion of aryl-azide block or gradient copolymers

Since the grafting could not be improved further by increasing the AzPh-PSar concentration or irradiation time, we decided to introduce more aryl-azide groups per polymer chain. For this poly(2-oxazoline) based block and pseudo gradient copolymers were prepared. Poly(2-oxazoline)s have gained great interest as biomaterial in the last years,[21,24] in particular the hydrophilic poly(2-methyl-2-oxazoline) (PMeOx) that features properties similar to PSar and PEG. More importantly though, monomers containing the aryl-azide group are synthetically readily accessible.[25] A small fraction of such an aryl-azide containing monomer, 2-(4-azidophenyl)-2-oxazoline (AzPhOx), was copolymerized with MeOx, enough to ensure multiple attachment points, but without significantly diminishing the copolymers hydrophilicity (Table 1). Also the spatial distribution was varied by either introducing AzPhOx as a block or by mixing it with MeOx to obtain a pseudo gradient distribution in the polymer. Despite increasing the aryl azide content, all poly(2-oxazoline)s were readily soluble in methanol (c > 50g/L), allowing the utilization of the same coating process as used for AzPh-PSar.

Poly(2-oxazoline) containing only one aryl azide unit (P(AzPhOx)$_1$-co-(MeOx)$_{100}$) showed similar results as AzPh-PSar. The water contact angles of OTS monolayers grafted with

P(AzPhOx)$_1$-*co*-(MeOx)$_{100}$ dropped only to 82°. As predicted, increasing the aryl azide content within the poly(2-oxazoline) chains led to a more efficient grafting of OTS monolayers (Table 1), and PP and PLA substrates ((PP: 103°→75°; PLA: 67°→ 56°; 20 g/L P[(AzPhOx)$_5$-*co*-(MeOx)$_{10}$]-*b*-(MeOx)$_{90}$). Interestingly though, the best performances were observed with the pseudo gradient copolymer P[(AzPhOx)$_5$-*co*-(MeOx)$_{10}$]-*b*-(MeOx)$_{90}$ and not with the block copolymer P(AzPhOx)$_5$-*b*-(MeOx)$_{100}$. It seems that more flexibility between the aryl-azide moieties facilitates multiple attachments to the surface rather than enhanced orientation of the chains towards the surface due to pronounced amphiphilicity. Already a single coating step with P[(AzPhOx)$_5$-*co*-(MeOx)$_{10}$]-*b*-(MeOx)$_{90}$ at half the polymer concentration surpassed the best coating results of polymers with a single aryl azide group. With further coating steps water contact angles as low as 33 ± 12° could be achieved. In contrast, the thickness of the grafted polymer layer increased only marginally with additional coating steps (Table 1). This indicates that rather than grafting layer on top of the previous layer the repetition increases the grafting density. Grafted polymer layer thicknesses of around 10 nm were also corroborated by atomic-force microscopy (AFM, Figure 2C). Moreover, XPS analysis confirmed the presence of poly(2-oxazoline) on the surfaces of PP (Figure 2) and PLA substrates (Figure S1).

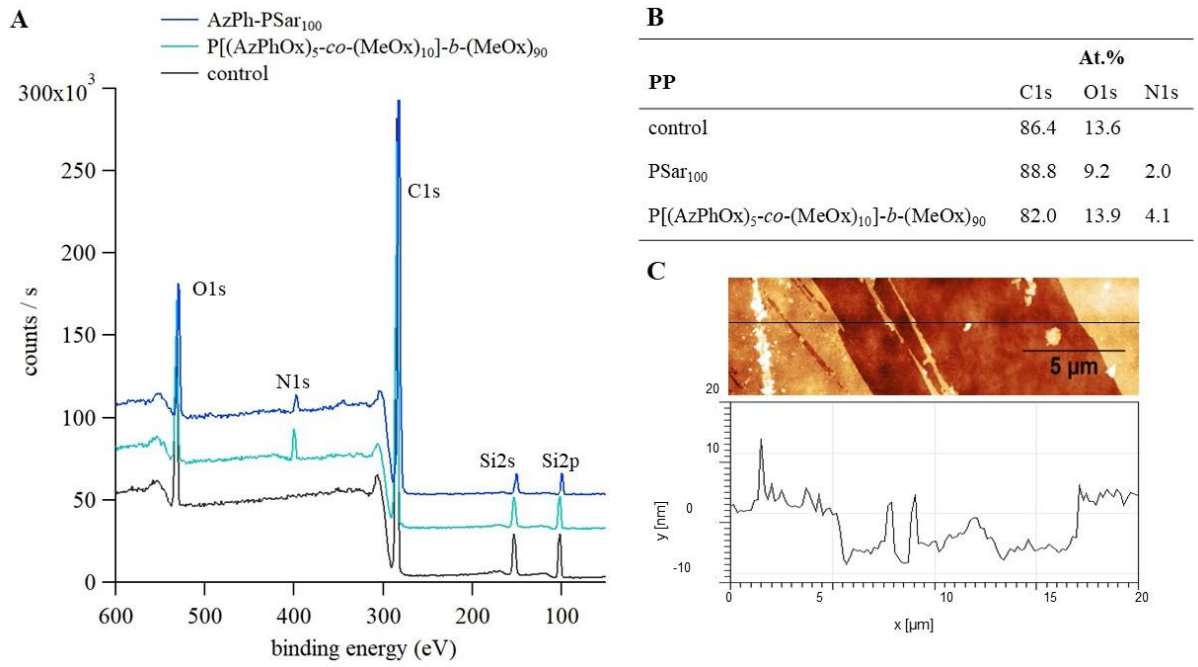

Figure 2. XPS full spectrum of PP substrates (A) and the atomic percentage (B). AFM height scan and corresponding height profile of P[(AzPhOx)$_5$-*co*-(MeOx)$_{10}$]-*b*-(MeOx)$_{90}$ grafted onto an OTS monolayer (C).

2.3 Versatility and stability of the surface modification

To visualize the coating process, P[(AzPhOx)$_5$-*co*-(MeOx)$_{10}$]-*b*-(MeOx)$_{90}$ was labeled with the fluorescence dye Rhodamine B (**Figure S2**), and grafted onto various polymer substrates to investigate its versatility (**Figure 3**). In addition, the coated surfaces were submerged in 100°C hot water for 15h to test the thermal stability of the surface functionalization. While PP, PLA, polyethylene terephthalate (PET, vascular graft) and polyurethane (PU, percutaneous nephrostomy catheter) were homogeneously coated with the grafted polymer chains and did not suffer any significant loss of the functionalization after the thermal treatment, we observed a scarce and blotchy distribution on silicone, which was almost completely removed after 15h in boiling water (**Figure S3**). The lack of a comprehensive surface functionalization was attributed to the poor wettability of the silicone substrate with the methanolic P[(AzPhOx)$_5$-*co*-(MeOx)$_{10}$]-*b*-(MeOx)$_{90}$ solution. It remains unclear though if that also caused the failed covalent attachment or if the materials itself is unsuitable for the procedure.

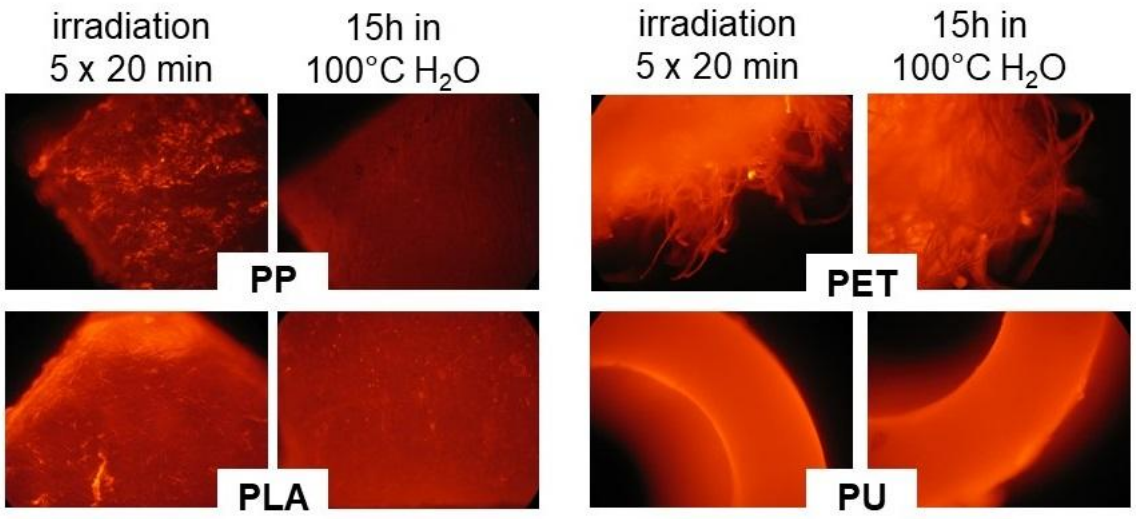

Figure 3. Visualization of the grafting process after five coating steps and its thermal stability in 100°C hot water by utilizing a fluorescent labeled P[(AzPhOx)$_5$-*co*-(MeOx)$_{10}$]-*b*-(MeOx)$_{90}$ copolymer on various materials.

To corroborate the indication of covalent attachment due to the presence of aryl-azide groups and to rule out generation of radicals on the substrates surface itself during UV-irradiation, which could lead to covalent bonds between the polymer chains and the surface, we repeated the experiments with a Rhodamine B labeled PMeOx homopolymer and P[(AzPhOx)$_5$-*co*-(MeOx)$_{10}$]-*b*-(MeOx)$_{90}$ with deactivated aryl azide groups (60 min UV irradiation of the polymer solution prior grafting). While PMeOx does not bind to the surface, the inactivated P[(AzPhOx)$_5$-*co*-(MeOx)$_{10}$]-*b*-(MeOx)$_{90}$ adheres marginally to PP and quite strongly to PLA (**Figure S4-5**). Thus the UV-active pseudo gradient copolymer is most likely not solely attached to the surfaces through covalent bonds alone but also through intermolecular forces.

2.4 Cytocompatibility and antibacterial activity of the modified surfaces

The cytocompatibility and antibacterial activity of the coated PP and PLA surfaces were tested. Cytocompatibility was tested via a cell proliferation assay (direct contact) with murine fibroblast cell line L929 (ISO 10993-5). The cells were allowed to adhere to the coated PP and PLA substrates for 3h. Subsequently the growth of the adhered cells was followed over 9d (**Figure 4A**). While none of the substrates performed as well as the tissue culture-treated

polystyrene (TCPS), the difference in cell proliferation on non-coated and coated substrates was either slightly improved (PP) by the coating or very similar (PLA). However, when the adherence of bacteria was tested significant changes were observed between the untreated and coated surfaces (Figure 4B). For both polymer substrates PP and PLA, the coating caused a drop of 2 to 3 orders of magnitude in the adherence of the reference bacteria strains *S. epidermidis* ATCC49461 and *E. coli* CFT073. This anti-adherence property of the coating lead to a strong reduction of biofilm formation (Figure 4C). In particular, biofilm formation on the grafted PLA substrates was almost completely impeded. This may be due to a higher coating density due to the additional adhesive interactions with the surface. These results are also in part seen in the anti-adherence data, but not as pronounced.

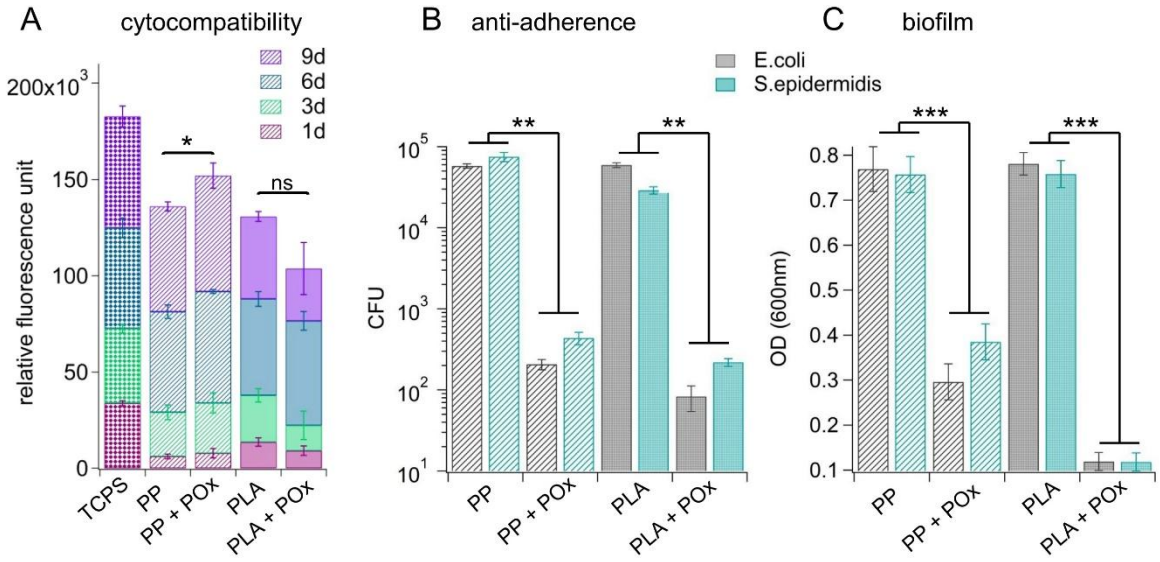

Figure 4. Effect of P[(AzPhOx)$_5$-*co*-(MeOx)$_{10}$]-*b*-(MeOx)$_{90}$ grafting onto PP and PLA substrates on cell proliferation of L929 mouse fibroblasts over 9d (n=5) (A), adherence after 24h (B) and biofilm formation after 72h (C) of *S. epidermidis* ATCC49461 and *E. coli* CFT073 bacteria. Data is represented as means±SD. Asterisks indicate statistical significance (t-test, ns p>0.5, *p<0.05, **p<0.01, ***p<0.001).

3. Conclusion

In conclusion, photoinsertion of rationally designed aryl-azide copolymers can be advantageously used for an efficient and direct modification of polymer surfaces. For the first time, thanks to a thorough evaluation of the macromolecular parameters, the importance of the spatial repartition of the photoreactive aryl-azide groups in the copolymer structure has been highlighted. The pseudo gradient copolymer enabled an efficient covalent grafting to introduce properties, herein antifouling properties, on chemically diverse polymer substrates. This strategy has a huge potential and could be implemented very easily in already existing value chains making this technology highly desirable for various industrial applications.

4. Experimental Section

Material and methods: All chemicals and materials were purchased from Sigma-Aldrich (St. Quentin Fallavier, France). 2-methyl-2-oxazoline and methyl triflate were distilled over CaH_2 before usage. Silicon wafers (type P/B, SSP, 0-100 ohm.cm, 335 µm thick) were ordered from UniversityWafer (Boston, USA). PET samples were cut off from a vascular graft (InterVascular Inc., 16W008, sample length 1-2 cm). PU samples were obtained from a percutaneous nephrostomy catheter (Rüsch, 340014, sample length 1-2 cm). Silicone samples were cut from suprapubic set (Rüsch, 170727, sample length 1-2 cm). Medical grade PP used for surgical mesh for hernia repair was obtained from Luxilon (Antwerp, Belgium). PLA was synthesized by bulk-ring opening copolymerization of L-lactide (92%) and DL-lactide (8%) (PURAC, Lyon, France) using tin 2-ethylhexanoate as catalyst. PLA and PP were pressed into 0.5-2 mm thick disks at 180°C and 5t for 30-45min using a Carver Manual Bench Top Laboratory Press and subsequently cut into squares (1 cm^2). NMR spectra were obtained

using an AMX300 Bruker spectrometer at room temperature (RT). The spectra were calibrated using the residual protonated solvent signals. Gel permeation chromatography (GPC) was performed on a GPC system consisting of a Waters 515 HPLC pump, Viscotek VE 7510 GPC degasser, 2x PLgel 5µm Mixed-D (300mm) columns and a UV-detector with dimethylformamid + 0.1% LiBr as eluent at a flow rate of 0.8 mL/min and PMMA as standards. Contact angles were captured with a CCD camera (Dataphysics OCAH200) and analyzed using ImageJ software. Optical fluorescence images were taken via an Axioskop Zeiss microscope (light intensity was kept constant). For cell culture experiment, murine fibroblast cell line L929, which are recommended by the International Standard Organization (ISO) committee as an *in vitro* biocompatibility test model (ISO 10993-5: Biological evaluation of medical devices, part 5: tests for *in vitro* cytotoxicity), were purchased from Sigma-Aldrich and grown at 37°C in 5% CO_2 incubator, in DMEM high glucose (Sigma-Aldrich) supplemented with 5% fetal bovine serum (Gibco), 2mM L-glutamine (Gibco) and 100 units per ml of penicillin-streptomycin (Sigma-Aldrich). Microplate reader CLARIOstar® (BMG Labtech) was used to assess cell viability via fluorescence intensity measurement thanks to Prestoblue® cell viability reagent (Invitrogen, A13261).

Monomer synthesis: The synthesis of sarcosine-*N*-carboxyanhydride was adapted from Fetsch et *al*.[26] A yield of 1.63 g (62%) sarcosine-*N*-carboxyanhydride as white powder was obtained. ^{1}H NMR (300 MHz, DMSO-d_6, δ): 4.22 (s, 2H, CH_2), 2.86 (t, 3H, CH_3) (**Figure S6**).

2-(4-azidophenyl)-oxazoline was synthesized as described by Binder and Gruber.[25] A yield of 2.49 g (44%) 2-(4-azidophenyl)-oxazoline as a yellow-brown powder was obtained. ^{1}H NMR (300 MHz, DMSO-d_6, δ): 7.88 (d, 2H, J = 8.7 Hz, Ar H), 7.20 (d, 2H, J = 8.7 Hz, Ar H), 4.39 (t, 2H, J = 9.3 Hz, CH_2), 3.94 (t, 2H, J = 9.3 Hz, CH_2) (**Figure S7**).

Polymerization of polysarcosine: First an initiator stock solution with 4-azido-aniline hydrochloride (AzPh, c=0.09M) and triethyl amine (TEA, c=0.24M) in dry benzonitrile was prepared. Appropriate amounts of the initiator stock solutions were added to sarcosine-NCA dissolved in dry benzonitrile (c~ 10 mg/mL). The reaction mixture was stirred at RT between 12h and 7d depending on the degree of polymerization. The polymer was precipitated twice in cold diethyl ether (10-20 fold of volume of polymer solution). After removal of the solvent and drying, the polymer was redissolved in H_2O and lyophilized.

AzPh-PSar$_{10}$: 4.5 mL of the initiator solution (n_{AzPh}=0.405 mmol, n_{TEA}=1.08 mmol) were added to 0.47 g sarcosine-NCA (n=4.08 mmol) and 1 mL dry benzonitrile. 223 mg (77%) of a dark brown powder was obtained.

GPC (DMF) 5.4 kg/mol, Đ= 1.3 (**Figure S10**); ATR-FTIR: ν = 2940 (m; $\nu_{as}(CH_3)$), 2120 (m, $\nu_{as}(N_3)$), 1640 (s, ν (CO) amide I), 1490 (s, $\delta_{as}(CH_3)$), 1401 (s, $\delta_s(CH_3)$), 1227 (s, ν (C-N)), 1100 (s, ν (C-N)), 842 cm^{-1} (s, ν (C-C)); ^{1}H NMR (300 MHz, D_2O, δ): 7.51 (bs, 2H, Ar H), 7.18 (bs, 2H, Ar H), 4.53-4.23 (m, 115H, CH_2), 3.12-2.94 (m, 172H, CH_3) (**Figure S8**); polymer structure by NMR: $PSar_{58}$, M_{NMR}= 4.1 kg/mol.

AzPh-PSar$_{100}$: 0.22 mL of the initiator solution (n_{AzPh}=0.02 mmol, n_{TEA}=0.053 mmol) were added to 0.23 g sarcosine-NCA (n=2.01 mmol) and 2.3 mL dry benzonitrile. 131 mg (92%) of a yellow powder was obtained.

GPC (DMF) 7700 g/mol, Đ= 1.2 (**Figure S10**); ATR-FTIR: ν = 2940 (m; $\nu_{as}(CH_3)$), 2120 (w, $\nu_{as}(N_3)$), 1640 (s, ν (CO) amide I), 1490 (s, $\delta_{as}(CH_3)$), 1401 (s, $\delta_s(CH_3)$), 1227 (s, ν (C-N)), 1100 (s, ν (C-N)), 842 cm^{-1} (s, ν (C-C)); ^{1}H NMR (300 MHz, D_2O, δ): 7.51 (bs, 2H, Ar H), 7.19 (bs, 2H, Ar H), 4.53-4.18 (m, 256H, CH_2), 3.13-2.94 (m, 385H, CH_3) (**Figure S9**); polymer structure by NMR: AzPh-$PSar_{128}$, M_{NMR}= 9.1 kg/mol.

Polymerization of poly(2-oxazoline) pseudo-gradient copolymers: An adequate amount of 2-(4-azidophenyl)-oxazoline was added to an evacuated flask and dried further under high vacuum. The initiator methyl triflate (MeOTf, 1eq), and dry benzonitrile were also added under inert conditions. In case of the pseudo gradient copolymer, the first block of 2-(4-azidophenyl)-oxazoline was copolymerized with part of the 2-methyl-2-oxazoline (MeOx). The reaction mixture was then stirred for 3d at 80°C. Next (the remaining) MeOx was added under argon flow to the reaction mixture. The polymerization was carried out for another day at 80°C. The reaction was terminated with 3 eq 1-BOC-piperazine, which was stirred for 5h at 40°C. Subsequently an excess of potassium carbonate was added and the mixture stirred over night at RT. After centrifugation and filtration, the solvent was removed and the residue dissolved in a mixture of chloroform and methanol (1/2, v/v) followed by precipitation in cold diethyl ether (10-20 fold of volume of polymer solution). After a second precipitation the polymer was dried, dissolved in H_2O and lyophilized. Yellow powders were obtained.

P[(AzPhOx)$_5$-co-(MeOx)$_{10}$]-b-(MeOx)$_{90}$: 17µL MeOTf (n=0.16 mmol), 99.8 mg AzPhOx (n=0.53 mmol), 0.09 mL MeOx (n=1.06 mmol), 0.80 mL MeOx (n= 9.4mmol), 58.1 mg 1-BOC-piperazine (n=0.31 mmol) and 5 mL benzonitrile. 1.05 g (99%) of a yellow powder was obtained.

GPC (DMF) 7.8 kg/mol, Đ= 1.3 (**Figure S13**); ATR-FTIR: ν = 2942 (m; $\nu_{as}(CH_3)$), 2126 ((w, $\nu_{as}(N_3)$), 1633 (s, ν (CO) amide I), 1421 (s, $\delta(CH_2\text{-}CO)$), 1258 (m), 1031 cm^{-1} (m); ^{1}H NMR (300 MHz, MeOD, δ): 7.89-7.19 (m, 13H, Ar H), 3.63-3.56 (m, 382H, N-CH_2-CH_2), 3.11-3.07 (m, 3H, CH_3^{Ini}), 2.77 (bs, 5H, H^{Pip}), 2.40-1.92 (m, 288H, CO-CH_3), 1.49 (bs, 8H, CH_3^{BOC}) (**Figure S12**); polymer structure by NMR: *P[(AzPhOx)$_3$-co-(MeOx)$_n$]-b-(MeOx)$_m$, n+m=96;* M_{NMR}= 8.9 kg/mol.

*P(AzPhOx)$_5$-b-(MeOx)$_{100}$:*17µL MeOTf (n=0.16 mmol), 98.9 mg AzPhOx (n=0.53 mmol), 0.89 mL MeOx (n=10.5 mmol), 61.5 mg 1-BOC-piperazine (n=0.33 mmol) and 5 mL benzonitrile. 0.94 g (94%) of a yellow powder was obtained.

GPC (DMF) 8.3 kg/mol, Đ= 1.3 (**Figure S13**); ATR-FTIR: ν = 2937 (m; $\nu_{as}(CH_3)$), 2126 ((w, $\nu_{as}(N_3)$), 1626 (s, ν (CO) amide I), 1416 (s, $\delta(CH_2\text{-}CO)$), 1241 (m), 1031 cm^{-1} (m); ^{1}H NMR (300 MHz, MeOD, δ): 7.88-7.19 (m, 16H, Ar H), 3.64-3.56 (m, 423H, N-CH_2-CH_2), 3.11-3.07 (m, 3H, CH_3^{Ini}), 2.79 (bs, 4H, H^{Pip}), 2.25-1.93 (m, 318H, CO-CH_3), 1.49 (bs, 8H, CH_3^{BOC}) (**Figure S11**); polymer structure by NMR: *P(AzPhOx)$_4$ -b-(MeOx)$_{106}$*; M_{NMR}= 10.0 kg/mol.

Polymerization of aryl-azide chain-end monofunctional poly(2-oxazoline): 119.2 mg AzPhOx was added to an evacuated flask and dried further under high vacuum. 14µL MeOTf (n=0.13 mmol), 0.54 mL MeOx (n=6.35 mmol) and 4 mL anhydrous acetonitrile were also added under inert conditions. The reaction mixture was then stirred for 1d at 80°C and terminated with 70.9 mg 1-BOC-piperazine (n=0.38 mmol), which was stirred for another 7h at 40°C. Subsequently an excess of potassium carbonate was added and the mixture stirred over night at RT. After centrifugation and filtration, the solvent was removed and the residue dissolved in a mixture of chloroform and methanol (1/2, v/v) followed by precipitation in cold diethyl ether (10-20 fold of volume of polymer solution). The polymer was dried, dissolved in H_2O and lyophilized. 0.33 g (50%) of a light yellow powder was obtained.

P(AzPhOx)$_1$-co-(MeOx)$_{100}$: GPC (DMF) 5.9 kg/mol, Đ= 1.3; ^{1}H NMR (300 MHz, MeOD, δ): 7.84-7.17 (m, 5H, Ar H), 3.60-3.36 (m, 385H, N-CH_2-CH_2), 3.07 (m, 3H, CH_3^{Ini}), 2.34-1.89 (m, 287H, CO-CH_3), 1.46 (bs, 7H, CH_3^{BOC}) (**Figure S14**); polymer structure by NMR: *P(AzPhOx)$_1$ -b-(MeOx)$_{96}$*; M_{NMR}= 8.6 kg/mol.

Fluorescent labeling of poly(2-oxazoline): First the end group 1-Boc-piperazine of P[$(AzPhOx)_5$-*co*-$(MeOx)_{10}$]-*b*-$(MeOx)_{90}$ was deprotected in a TFA/MeOH (1/1, v/v) solution (c~75 mg/mL) for 30min at room temperature. After removal of the solvent under high vacuum, the residue was dissolved in H_2O_{dd}, dialysed (MWCO=3.5kDa) for 2h and lyophilized. The deprotected polymer was then dissolved in anhydrous DMF (c=0.1mg/µL) and coupled with a 1.2 fold excess of Rhodamine B isothiocyanate (RBITC) and 1 eq diisopropylethylamine as base. The reaction mixture was shaken for 3d in the dark at 37°C. Excess dye was removed via dialysis. For this the reaction mixture was diluted with a 15 fold excess of H_2O_{dd} and transferred into a dialysis bag (MWCO=1kDa). After 4d the dialysis was stopped and the polymer lyophilized. Degree of labeling was obtained spectrophotometrically and was found for the UV-active copolymer at 20.1%, and for the PMeOx homopolymer at 24%.

OTS monolayer: Silicon wafers were degreased with $CHCl_3$ in ultrasonic bath for 30min and subsequently immerged in 100°C hot piranha solution (4/1 H_2SO_4/H_2O_2, v/v) which was gently stirred. After 2h the silicon wafers were washed with H_2O_{dd}, rinsed with ethanol and dried with Ar-flow. The pieces were separately incubated with an OTS solution (2.5 mM in 4/1 hexadecane/$CHCl_3$, v/v) at 17°C over night. After removal of the OTS solution, the samples were washed with $CHCl_3$ in ultrasonic bath for 20 min, rinsed again with $CHCl_3$ and dried with Ar-flow. Successful deposition of OTS monolayer was confirmed with water contact angle measurement (~105°).

Coating of surface: The aryl-azide containing polymers were dissolved in degassed methanol yielding concentrations of 10 and 20 g/L. Polymer substrate surfaces were washed prior modification for 15-30 min in methanol in ultrasonic bath and dried for another 15 min under high vacuum. The polymer solution was sprayed onto polymer substrates and OTS/silicon

surfaces, which were mildly heated to 60°C, using an airbrush. Subsequently the surfaces were irradiated for 20 min using a chromatography lamp VL-4C (254 nm, 8W) which was positioned 2-3 cm above the surfaces. After irradiation the surfaces were washed in methanol for 10 min. The procedure was repeated up to 5 times to improve the result. After the final irradiation step the surfaces were washed more extensively for 60 min and dried under high vacuum.

X-ray photoelectron spectrometry: XPS analyses were carried out on an ESCALAB 250 photoelectron spectrometer from Thermo Electron. Source type was the Al K_α X-ray at 1486.6 eV with an overall instrument resolution of 1.1 eV. The spectra were collected from a surface area of 400 μm^2 at an electron takeoff angle of 90° to the sample surface and calibrated to the binding energy of the C-C component of C_{1s} peak to 284.8 eV.

Ellipsometry: Multiple angle of incidence ellipsometry (Optrel, Germany; λ = 533 nm) was performed on several silicon wafers before and after each step of the surface functionalization. Incident angle was scanned from 70° to 80° in 2° steps. Results have been fitted using a single interfacial layer model. This approximation is justified by the fact that silica, OTS and the grafted polymer layer have approximately the same refractive index, nL=1.46. The thickness reported in Table 1 are calculated by subtracting the thickness of the OTS layer to the total thickness (OTS + grafted polymer layers).

Atomic-force microscopy: AFM studies were carried out on a Nanoman atomic force microscope (Veeco Metrology, Santa Barbara, CA) equipped with a closed loop and run by Nanoscope 5 software (Bruker Instrument). Using an NCL cantilever (Nanosensors, Neuchatel, Switzerland) images were taken in tapping mode under ambient conditions. Images were analyzed via Gwyddion 2.31 software.

Cell proliferation assay: The coated and non-treated PP and PLA substrates were cleaned with 70% ethanol and submerged in PBS containing 10% penicillin/streptomycin over night and finally washed with PBS. The decontaminated surfaces were placed into a 24-well plate. $2x10^5$ L929 cells were seeded on each substrate maintained in the wells via a Teflon ring. Tissue culture-treated polystyrene (TCPS) was used as a positive control. After 3h incubation at 37°C and 5% CO_2 to allow adherence of the cells, the surfaces were washed with PBS and 1 mL/well culture medium was added. After defined points of time, incubation was stopped, cell culture medium exchanged with medium containing 10% PrestoBlue® (Invitrogen, A13261), incubated for 30min and the supernatants fluorescence at 590 nm measured. By adding fresh culture medium again to the surfaces, cell growth was followed over multiple days (1, 3, 6, and 9).

*Bacterial strains:*The clinical bacterial strains *Staphylococcus epidermidis* ATCC49461 and *Escherichia coli* CFT073 were used. Before commencing the antibacterial *in vitro* tests, the bacterial strains were aerobically grown overnight on Muller Hinton medium at 37°C under stirring.

Anti-adherence study: The polymer substrates were submerged in a bacterial solution (OD_{600}=0.05). After 1h the substrates were rigorously washed 3 times with sterilized water and subsequently immerged in neutral medium for 24h at 37°C under static conditions. The adhered bacteria were recovered by vortexing and sonication of the substrates in neutral saline. Bacteria were quantified by serial dilution and spread plating on Mueller-Hinton agar. Strongly adhered bacteria were detached by dipping the substrate onto the surface of Mueller-Hinton agar plates about 15 times. Colony counts were carried out after incubation at 37°C over night. Total bacterial adherence was calculated by adding the colony forming unit (CFU)

counts of all cultivated bacteria. Bacteria were verified by Maldi-Tof analysis (Vitek-MS, BioMérieux).

Biofilm study: The polymer substrates were submerged in wells containing the various bacterial strains diluted in culture medium (OD_{600}=0.05). After 72h at 37°C the substrates were removed from the wells, rinsed vigorously with sterile water and incubated for 10min in 0.1% crystal violet solution. Excess dye was removed by washing the samples 3 times with sterile water. The bacteria are then precipitated with 250µL DMSO. The obtained solution was spectrophotometrically analyzed to measure the OD_{600}.

Supporting Information
Supporting Information is available from the Wiley Online Library or from the author.

Acknowledgements
The authors wish to thank University of Montpellier (UM1 7th Post-doctoral Fellowship Program) and French Embassy in Germany-Department for Science (French-German Post-doctoral action 2015) for A.S.'s fellowship, Valérie Flaud for the XPS analyses, Michel Ramona for the AFM analyses and Prof. Rainer Jordan for his advice.

Received: ((will be filled in by the editorial staff))
Revised: ((will be filled in by the editorial staff))
Published online: ((will be filled in by the editorial staff))

References

[1] T. R. Garrett, M. Bhakoo, Z. Zhang, *Prog. Nat. Sci.* **2008**, *18*, 1049.

[2] J.M. Schierholz, J. Beuth, *J. Hosp. Infect.* **2001**, *49*, 87.

[3] R. O. Darouiche, *Clin. Infect. Dis.* **2001,** *33*, 1567.

[4] J. Hasan, R. J. Crawford, E. P. Ivanova, *Trends Biotechnol.* **2013**, *31*, 295.

[5] Z.K. Zander, M.L. Becker, *ACS Macro Lett.* **2018**, *7*, 16.

[6] Q. Lu, E. Danner, J. H. Waite, J. N. Israelachvili, H. Zeng, D. S. Hwang, *J. R. Soc. Interface* **2012**, *10*, 20120759.

[7] K. Chawla, S. Lee, B. P. Lee, J. L. Dalsin, P. B. Messersmith, N. D. Spencer, *J. Biomed. Mater. Res. A* **2009**, *3*, 742.

[8] C. Sardo, B. Nottelet, D. Triolo, G. Giammona, X. Garric, J.-P. Lavigne, G. Cavallaro, J. Coudane, *Biomacromolecules* **2014**, *15*, 4351.

[9] S. El Habnouni, J.-P. Lavigne, V. Darcos, B. Porsio, X. Garric, J. Coudane, B. Nottelet, *Acta Biomater.* **2013**, *9*, 7709.

[10] G. W. J. Fleet, R. R. Porter, J. R. Knowles, *Nature* **1969**, *224*, 511.

[11] A. Klip, C. Gitler, *Biochem. Biophys. Res. Communi.* **1974**, *60*, 1155.

[12] K. M. Abu-Salah, J. B. C. Findlay, *Biochem. J.* **1977**, *161*, 223.

[13] J. Zhang, Y. Liu,B. Yuan, Z. Wang, M. Schönhoff, X. Zhang, *Chem. Eur. J.* **2012**, *18*, 14968.

[14] E. Gérard, E. Bessy, C. Salvagnini, V. Rerat, M. Momtaz, G. Hénard, P. Marmey, T. Verpoort, J. Marchand-Brynaert, *Polymer* **2011**, *52*, 1223.

[15] A. J. Gross, S. S. C. Yu, A. J. Downard, *Langmuir* **2010**, *26*, 7285.

[16] V. Pourcelle, S. Devouge, M. Garinot, V. Préat, J. Marchand-Brynaert, *Biomacromolecules* **2007**, *8*, 3977.

[17] A. Ovsianikov, Z. Li, J. Torgersen, J. Stampfl, R. Liska, *Adv. Funct. Mater.* **2012**, *22*, 3429.

[18] A. Zhu, M. Zhang, J. Wu, J. Shen, *Biomaterials* **2002**, *23*, 4657.

[19] G. Li, H. Zheng, Y. Wang, H. Wang, Q. Dong, R. Bai, *Polymer* **2010**, *51*, 1940.

[20] C. Hadler, K. Wissel, G. Brandes, W. Dempwolf, G. Reuter, T. Lenarz, H. Menzel, *Mater. Sci. Eng. C* **2017**, *75*, 286.

[21] M. Barz, R. Luxenhofer, R. Zentel, M. J. Vicent, *Polym. Chem.* **2011**, *2*, 1900.

[22] M. Schneider, C. Fetsch, I. Amin, R. Jordan, R. Luxenhofer, *Langmuir* **2012,** *28*, 16099.

[23] S. Palzer, C. Hiebl, K. Sommer, H. Lechner, *Chem. Ing. Tech.* **2001**, *73*, 1032.

[24] R. Luxenhofer, Y. Han, A. Schulz, J. Tong, Z. He, A. V. Kabanov, R. Jordan, *Macromol. Rapid Commun.* **2012**, *33*, 1613.

[25] W. H. Binder, H. Gruber, *Macromol. Chem. Phys.* **2000**, *201*, 949.

[26] C. Fetsch, A. Grossmann, L. Holz, J. F. Nawroth, R. Luxenhofer, *Macromolecules* **2011**, *44*, 6746.

Photoinsertion of rationally designed aryl-azide copolymers is exploited for an efficient and direct surface modification of polymer surfaces. The photografting efficiency is discussed with respect to the macromolecular structures with a pseudo gradient copolymer giving highest efficacy. The versatility of the approach is illustrated with antifouling poly(2-oxazoline)-based copolymers to impart antibacterial properties to various clinically relevant polymer substrates.

A. Schulz, A. Stocco, A. Bethry, J.-P. Lavigne, J. Coudane, B. Nottelet*

Direct Photomodification of Polymer Surfaces: Unleashing the Potential of Aryl-Azide Copolymers

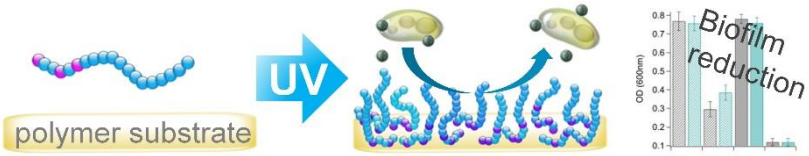

Supporting Information

Direct Photomodification of Polymer Surfaces: Unleashing the Potential of Aryl-Azide Copolymers

*Anita Schulz, Antonio Stocco, Audrey Bethry, Jean Philippe Lavigne, Jean Coudane, Benjamin Nottelet**

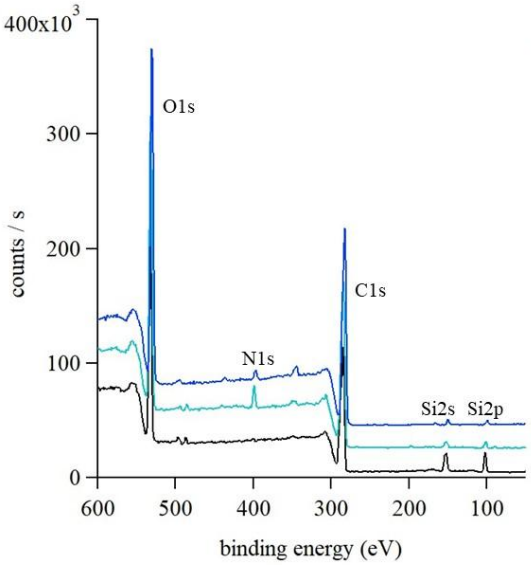

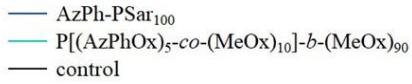

PLA	At.%		
	C1s	O1s	N1s
control	61.5	37.3	1.2
$PSar_{100}$	65.9	33.1	1.0
$P[(AzPhOx)_5\text{-}co\text{-}(MeOx)_{10}]\text{-}b\text{-}(MeOx)_{90}$	62.5	33.8	3.7

Figure S1. XPS full spectrum of PLA substrates and the corresponding atomic percentage.

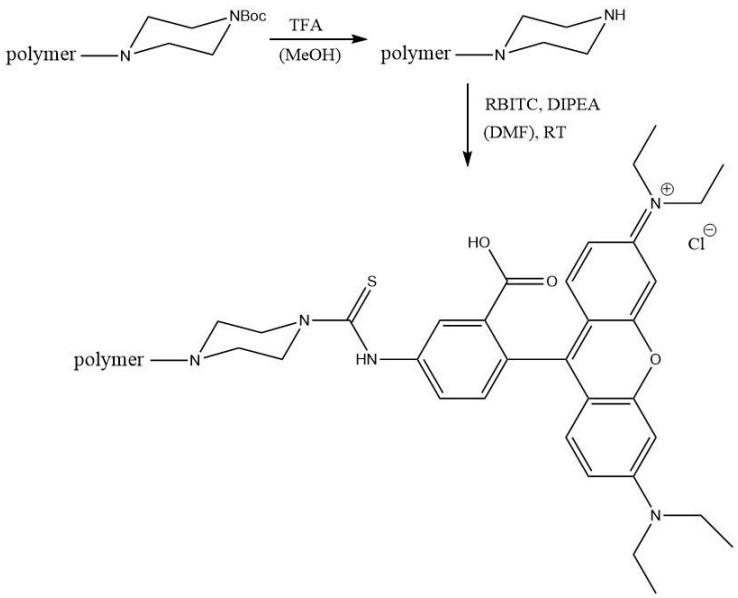

Figure S2. Fluorescent labeling of poly(2-oxazoline)s with Rhodamine B.

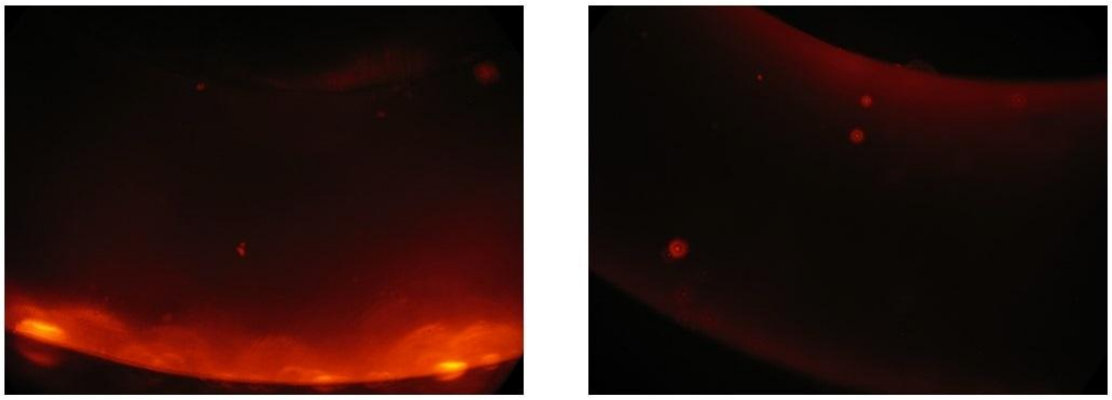

Figure S3. Visualization of the grafting process on a silicone catheter after five coating steps (left) and its thermal stability in 100°C hot water (right) by utilizing a fluorescent labeled P[(AzPhOx)$_5$-*co*-(MeOx)$_{10}$]-*b*-(MeOx)$_{90}$ copolymer.

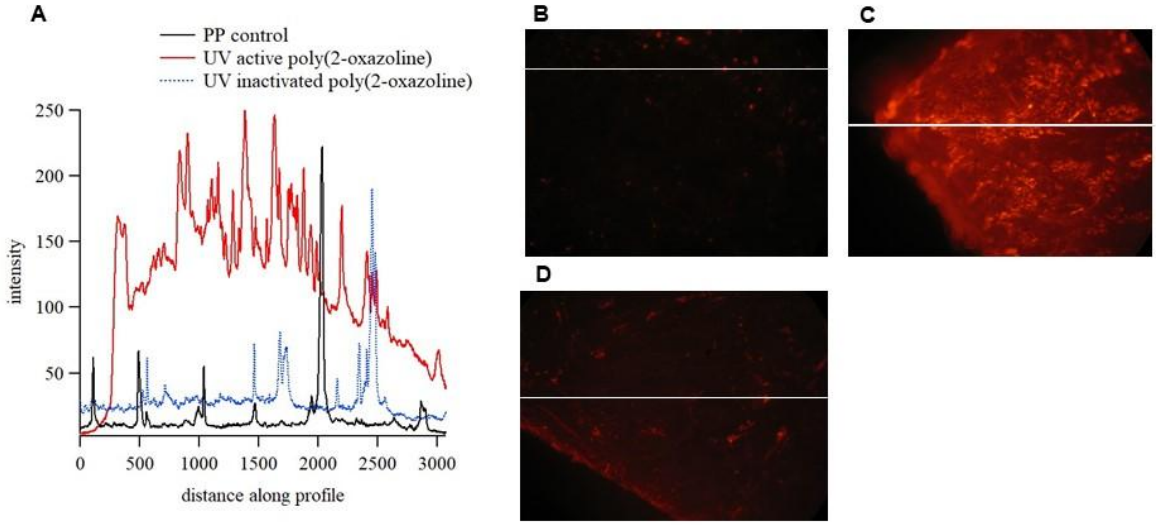

Figure S4. Line profiles of the individual red component along the specified path of all surface images shown (A). Fluorescence microscopy images of untreated PP surface (B), PP surface 5x irradiated for 20 min with UV active P[(AzPhOx)$_5$-*co*-(MeOx)$_{10}$]-*b*-(MeOx)$_{90}$ (C) and with UV inactivated P[(AzPhOx)$_5$-*co*-(MeOx)$_{10}$]-*b*-(MeOx)$_{90}$ (D).

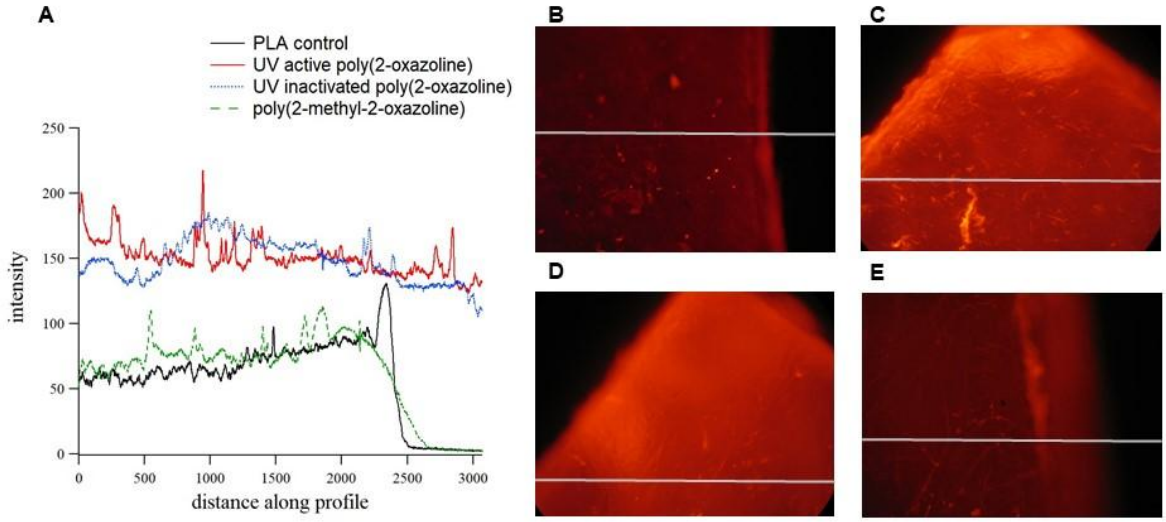

Figure S5. Line profiles of the individual red component along the specified path of all surface images shown (A). Fluorescence microscopy images of untreated PLA surface (B), PLA surface 5x irradiated for 20 min with UV active P[(AzPhOx)$_5$-*co*-(MeOx)$_{10}$]-*b*-(MeOx)$_{90}$ (C), with UV inactivated P[(AzPhOx)$_5$-*co*-(MeOx)$_{10}$]-*b*-(MeOx)$_{90}$ (D) and with PMeOx$_{60}$ (E).

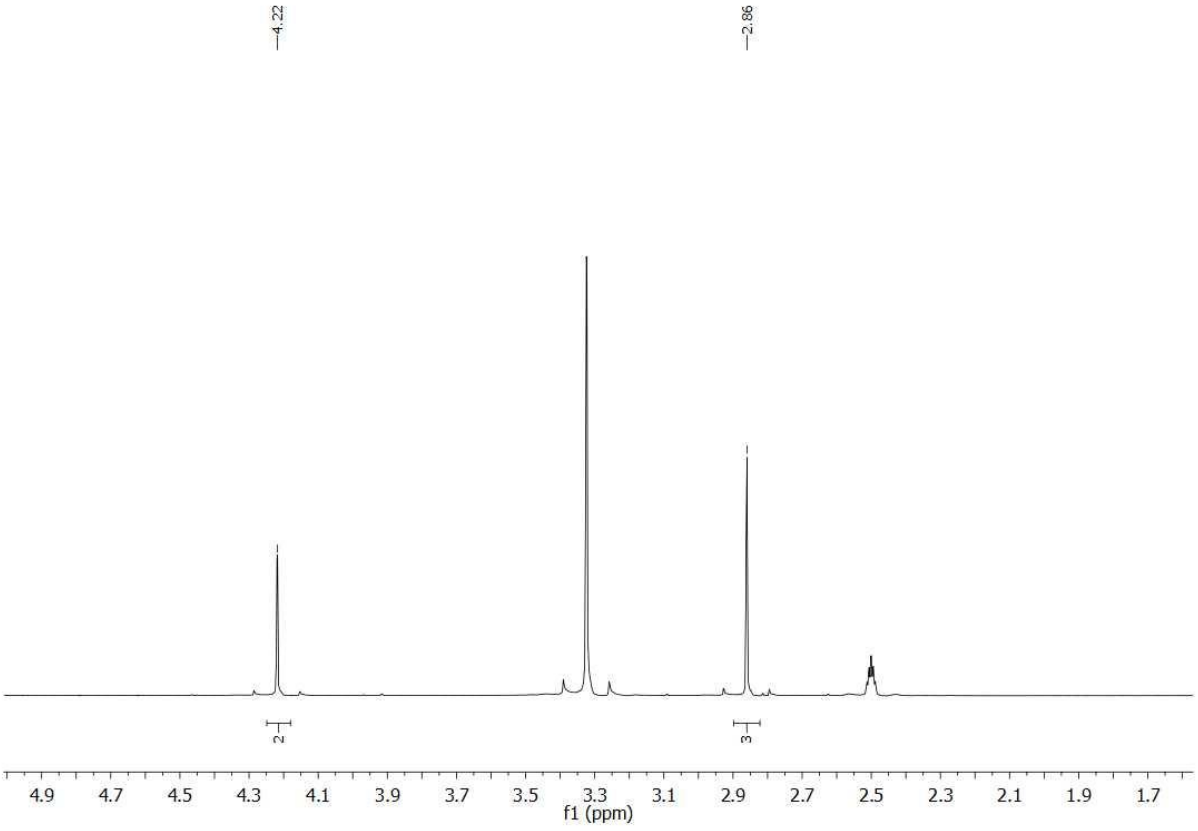

Figure S6. ^{1}H-NMR of sarcosine-*N*-carboxyanhydride in DMSO.

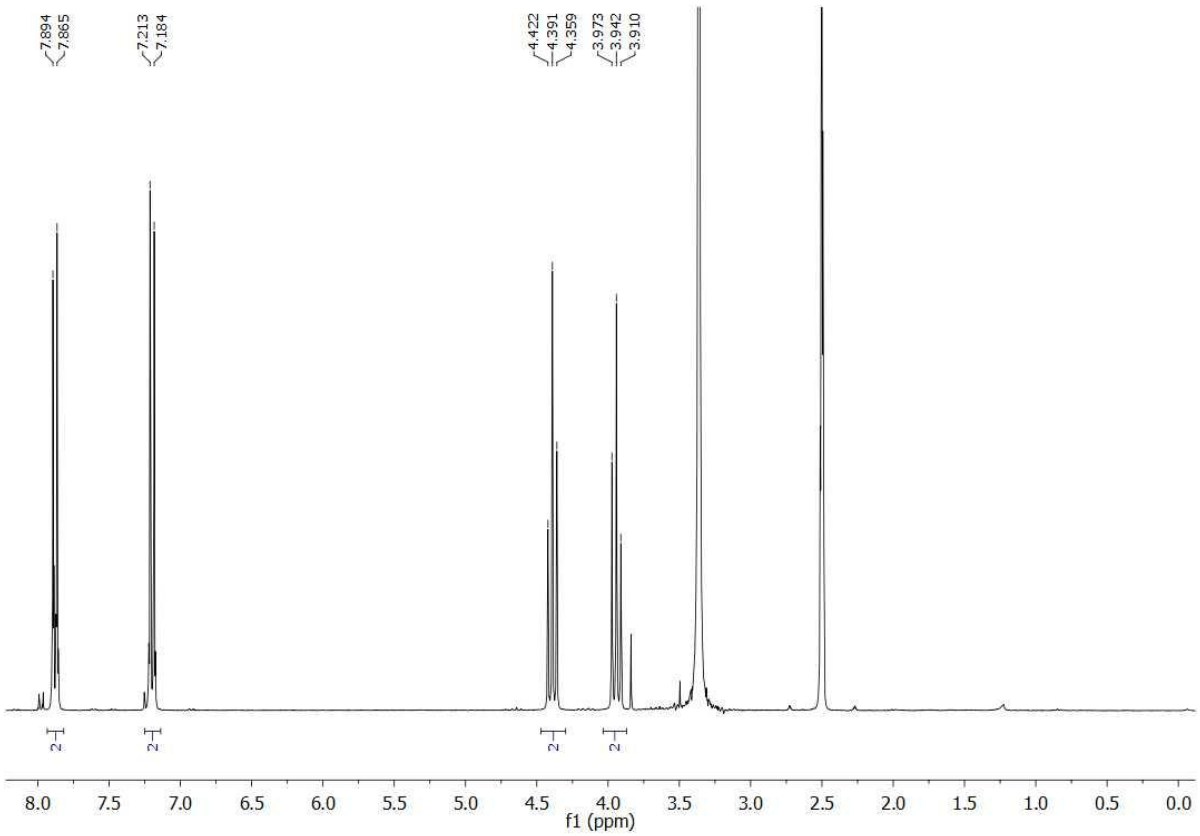

Figure S7. ^{1}H-NMR of 2-(4-azidophenyl)-oxazoline in DMSO.

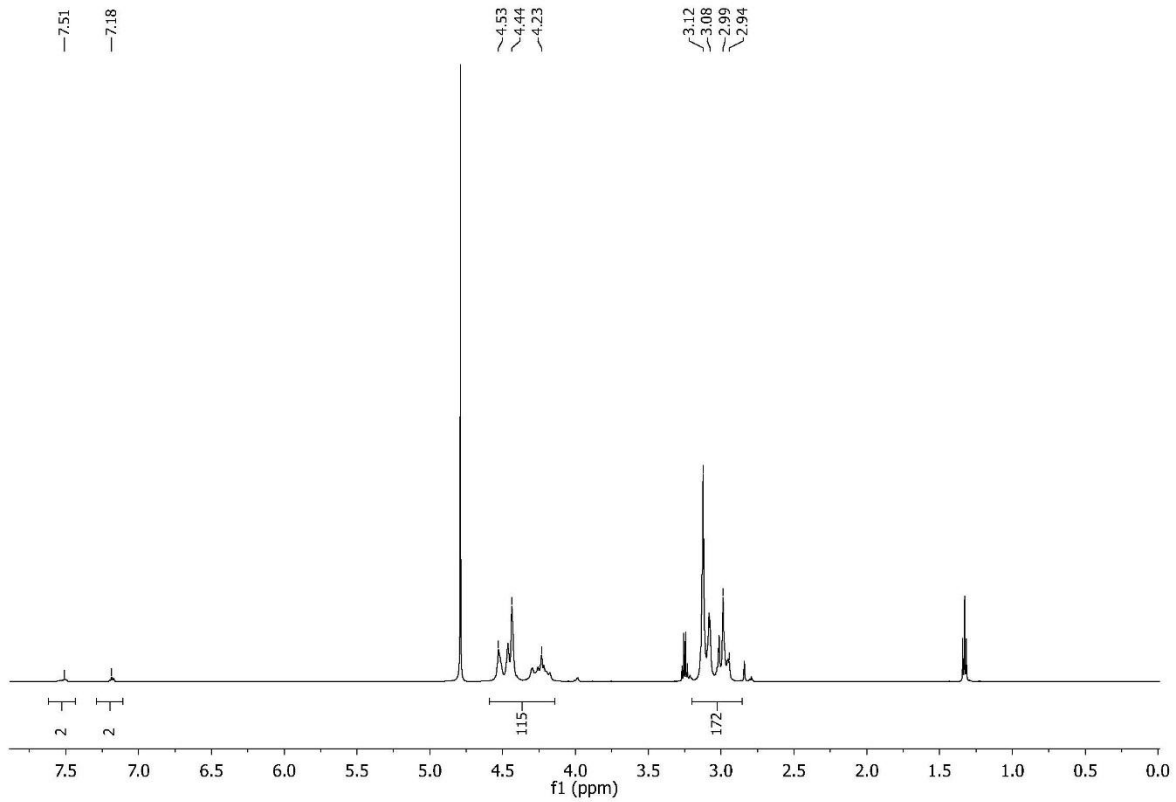

Figure S8. ^{1}H-NMR of AzPh-PSar10 in D_2O.

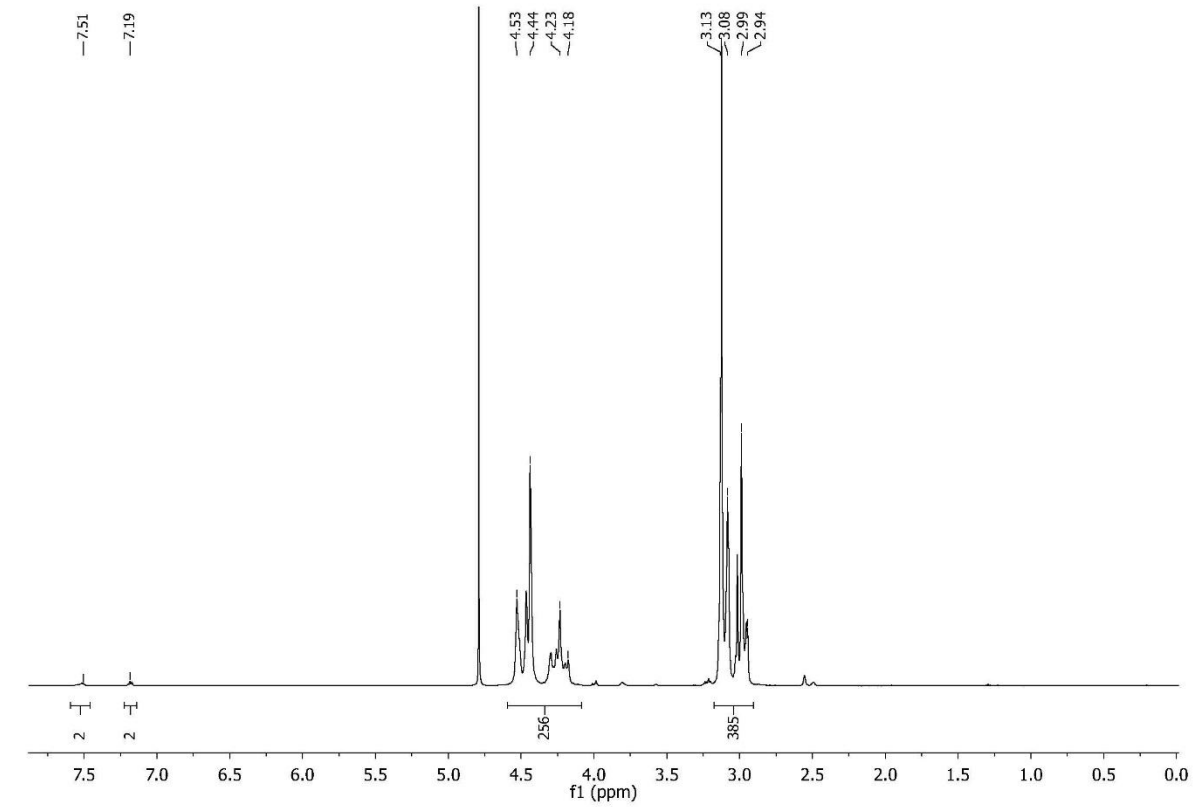

Figure S9. ^{1}H-NMR of AzPh-PSar$_{100}$ in D_2O.

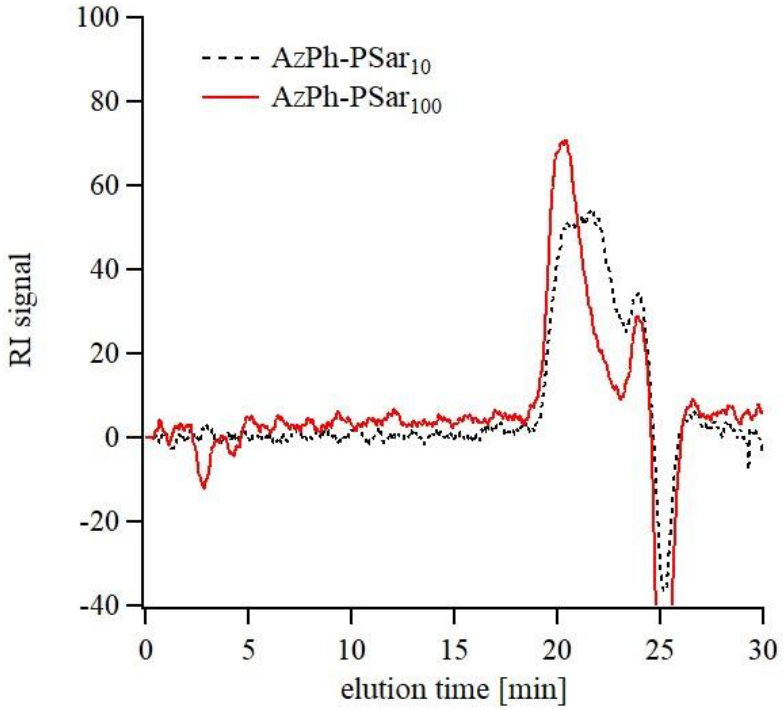

Figure S10. GPC elugram of AzPh-PSar in DMF.

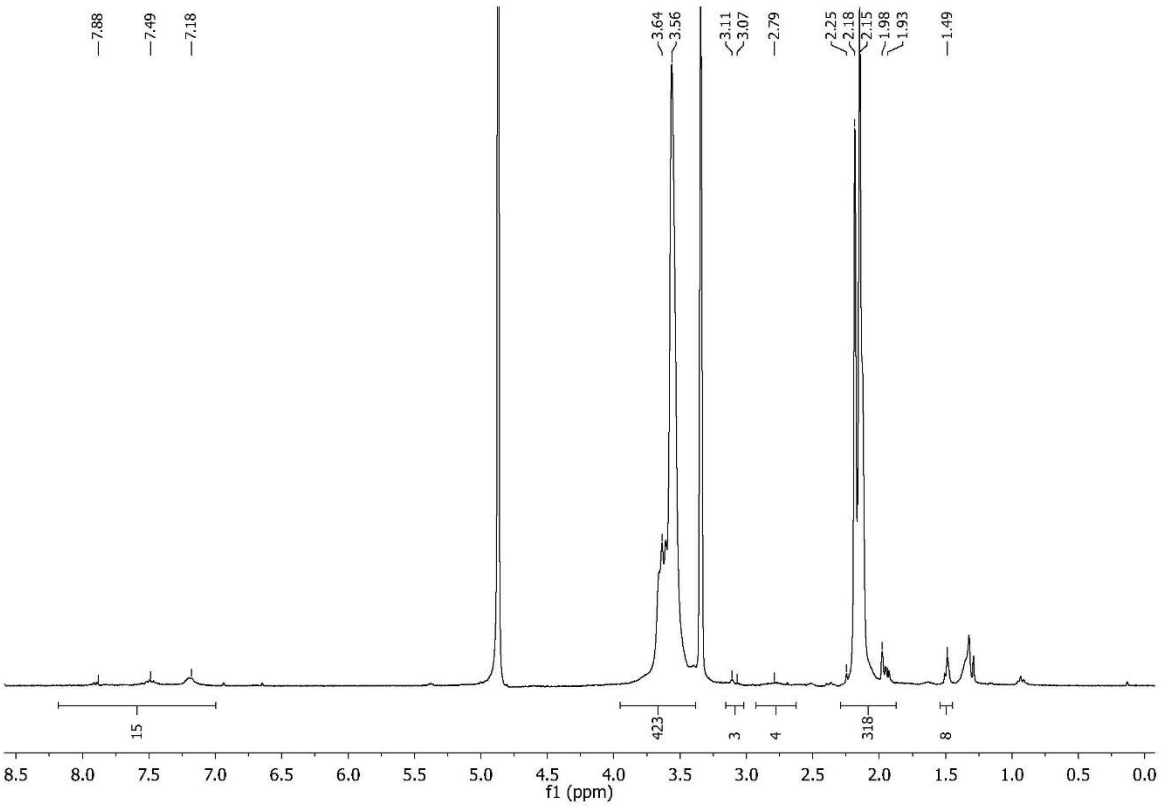

Figure S11. ^{1}H-NMR of P(AzPhOx)$_5$-*b*-(MeOx)$_{100}$ in MeOD.

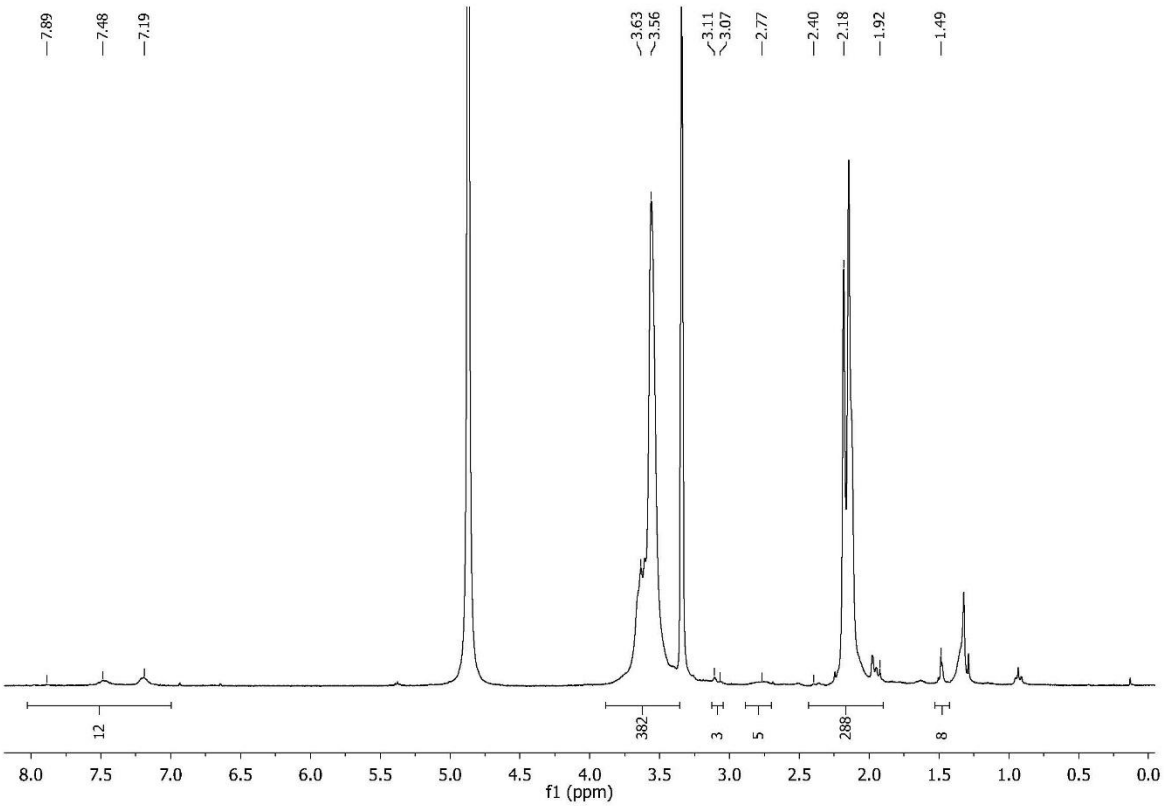

Figure S12. ^{1}H-NMR of P[(AzPhOx)$_5$-*co*-(MeOx)$_{10}$]-*b*-(MeOx)$_{90}$ in MeOD.

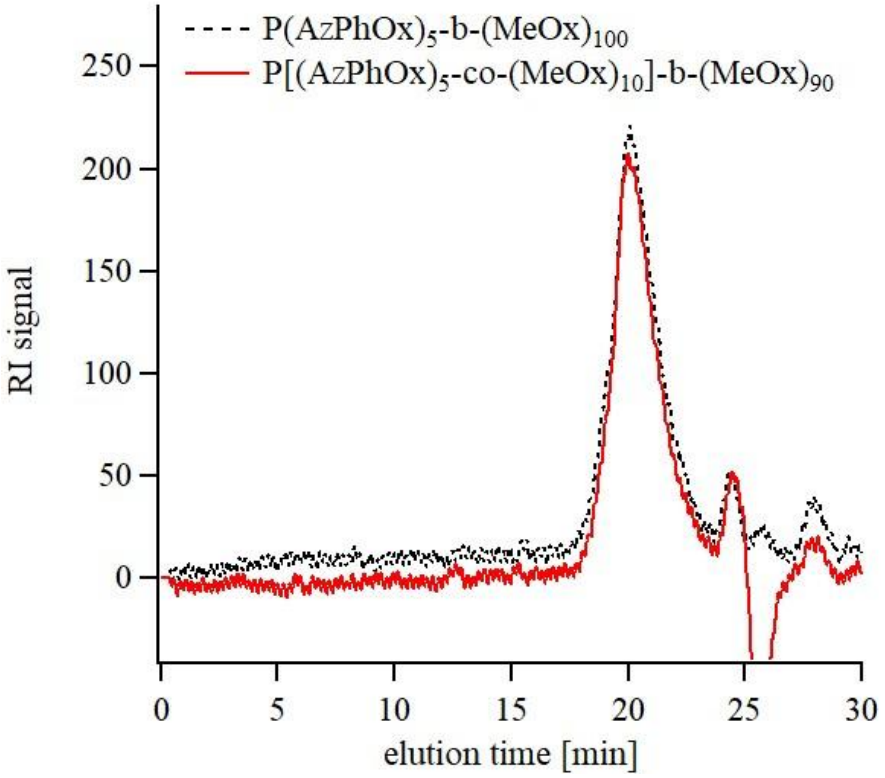

Figure S13. GPC elugram of poly(2-oxzaline) copolymers in DMF.

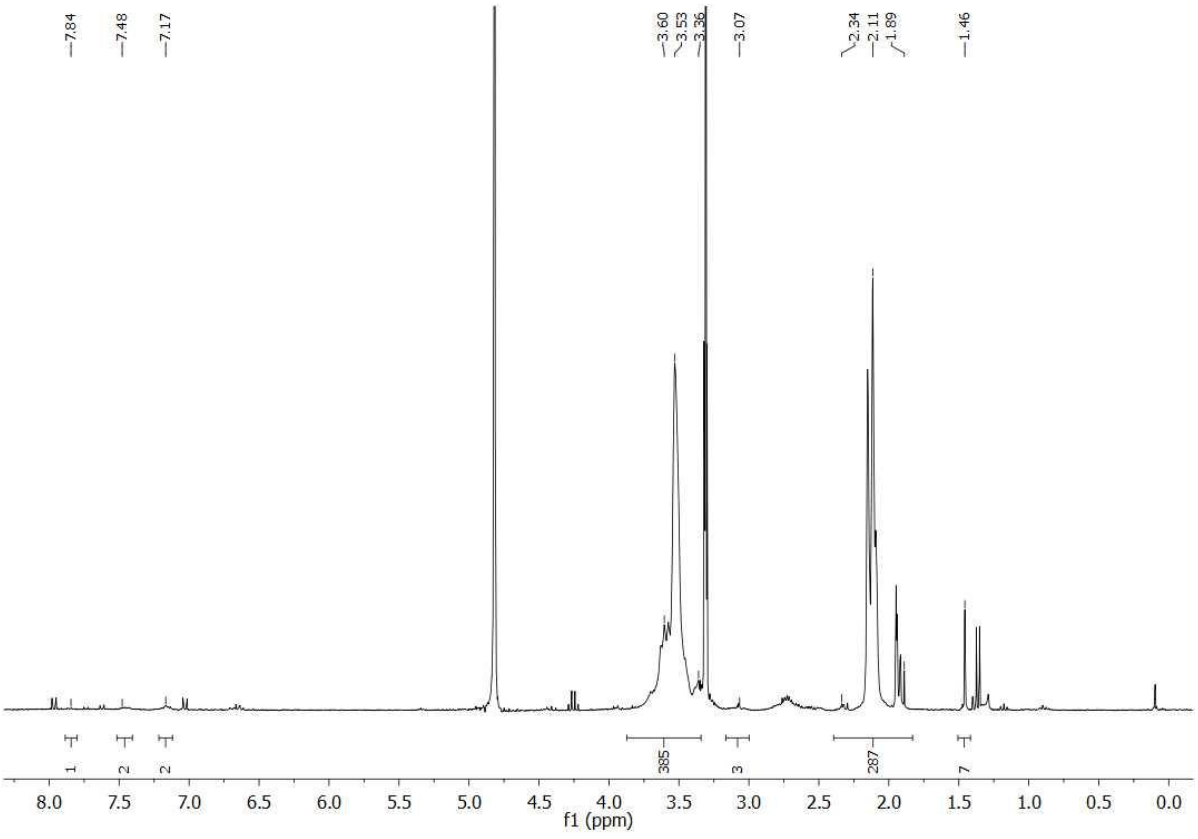

Figure S14. ^{1}H-NMR of P(AzPhOx)$_1$-*co*-(MeOx)$_{100}$ in MeOD.